



## Measurement of Human Urine Specific Gravity Using Nanoplasmonics: A Paradigm Shift from Scales to Biosensors

Bhalla, N. (2024). Measurement of Human Urine Specific Gravity Using Nanoplasmonics: A Paradigm Shift from Scales to Biosensors. *Advanced Sensor Research*, 3(4), 1-7. Article 2300115. Advance online publication. <https://doi.org/10.1002/adsr.202300115>

[Link to publication record in Ulster University Research Portal](#)

**Published in:**  
Advanced Sensor Research

**Publication Status:**  
Published online: 02/01/2024

**DOI:**  
[10.1002/adsr.202300115](https://doi.org/10.1002/adsr.202300115)

**Document Version**  
Publisher's PDF, also known as Version of record

**General rights**  
Copyright for the publications made accessible via Ulster University's Research Portal is retained by the author(s) and / or other copyright owners and it is a condition of accessing these publications that users recognise and abide by the legal requirements associated with these rights.

**Take down policy**  
The Research Portal is Ulster University's institutional repository that provides access to Ulster's research outputs. Every effort has been made to ensure that content in the Research Portal does not infringe any person's rights, or applicable UK laws. If you discover content in the Research Portal that you believe breaches copyright or violates any law, please contact [pure-support@ulster.ac.uk](mailto:pure-support@ulster.ac.uk).

# Measurement of Human Urine Specific Gravity Using Nanoplasmonics: A Paradigm Shift from Scales to Biosensors

Nikhil Bhalla


Urine Specific Gravity ( $U_{SG}$ ) is a direct indicator of the osmolarity of the urine and therefore it can be considered as a nonspecific marker of several underlying diseases which result in changes in hydration levels of the body. Here, a biosensor based on the principle of localized surface plasmon resonance (LSPR) is developed, which utilizes its refractive index sensing properties to measure  $U_{SG}$  with a sensitivity of  $79.21 \text{ nm } U_{SG}^{-1}$  unit. Additionally, the sensor can measure the serum protein content within the urine. Traditionally, handheld refractometers are used to measure  $U_{SG}$  which are operated as calibrated refractive index scales rather than a sensor. A simple experiment demonstrating the advantage of a sensor over scale, with LSPR as the transduction method, is also conducted to highlight the enhanced sensitivity of a sensor over a scale. Finally, analysis of results with an unsupervised machine learning algorithm, principal component analysis (PCA), demonstrate the feasibility of automating or perhaps adding artificial intelligence to such sensors, thereby exemplifying a potential paradigm shift from refractive index scales to sensors in  $U_{SG}$  measurement.

## 1. Introduction

Urine Specific Gravity ( $U_{SG}$ ) is a measure of the density of urine relative to water, and it reflects the concentration of dissolved substances in the urine.<sup>[1]</sup> In humans,  $U_{SG}$  ranges from 1.003 to 1.030, with an average of 1.020 for a normal hydrated body

N. Bhalla  
Nanotechnology and Integrated Bioengineering Centre (NIBEC)  
School of  
Engineering  
Ulster University  
2–24 York Street, Belfast BT15 1AP, UK  
E-mail: [n.bhalla@ulster.ac.uk](mailto:n.bhalla@ulster.ac.uk)

N. Bhalla  
Healthcare Technology Hub  
School of Engineering  
Ulster University  
2–24 York Street, Belfast BT15 1AP, UK

 The ORCID identification number(s) for the author(s) of this article can be found under <https://doi.org/10.1002/adsr.202300115>

© 2024 The Authors. Advanced Sensor Research published by Wiley-VCH GmbH. This is an open access article under the terms of the [Creative Commons Attribution](#) License, which permits use, distribution and reproduction in any medium, provided the original work is properly cited.

DOI: 10.1002/adsr.202300115

condition.<sup>[2]</sup> There are several clinical complications associated with the abnormal  $U_{SG}$ . For instance, when a person is dehydrated, their body conserves water by producing less urine which increases the concentration of waste products in the urine, resulting in a higher  $U_{SG}$ , and therefore the state of hydration can be assessed using  $U_{SG}$ .<sup>[3–5]</sup> In patients with kidney disease, the kidneys may not be able to concentrate urine properly, resulting in a lower  $U_{SG}$ .<sup>[6]</sup> It has also been reported that uncontrolled diabetes can lead to high blood glucose levels, which can cause glucose to spill into the urine.<sup>[5]</sup> Furthermore, the infections of the urinary tract can cause the  $U_{SG}$  to alter which might be due to the presence of white blood cells and other substances in the urine.<sup>[7–10]</sup>

$U_{SG}$  is currently measured using a handheld refractometer, which is a small device, see **Figure 1a**, that uses light to measure the refractive index of the urine.<sup>[11,12]</sup> The refractive index is then converted to  $U_{SG}$  value using a calibration chart or a digital display on the device.<sup>[13]</sup> In some cases,  $U_{SG}$  may also be measured using a dipstick test, which provides a rough estimate of the  $U_{SG}$ , based on the color change of a chemical indicator.<sup>[14,15]</sup> However, this method is less accurate than using a refractometer and is more commonly used for qualitative screening purposes.<sup>[16,17]</sup> While refractometers are routinely used in clinical settings for  $U_{SG}$  measurements, these are reported to be sensitive to humidity and temperature (leading to variation from measurement to measurement), which allows limited possibilities of point-of-use measurement, data logs and analysis, and transmission of the data to the healthcare setting.<sup>[18–20]</sup> This is due to the fact that these refractometers completely rely on the optical prism-based calibrated scales, which are sensitive to changes in the refractive index (RI) of the media.<sup>[21]</sup> These calibrated scales are not sensors as the measurements are based on visual observation of the scale.<sup>[22,23]</sup> This may introduce errors in the measurement due to the user's handling skills usually resulting from differences in the judgment from user to user. However, such errors or limitations can easily be addressed by electronic or optical sensors because in principle response from sensors is directly displayed rather than being read by a human eye. Additionally, apart from enhanced sensitivity and selectivity compared to the scales, data from sensors can easily be stored or transmitted to a database

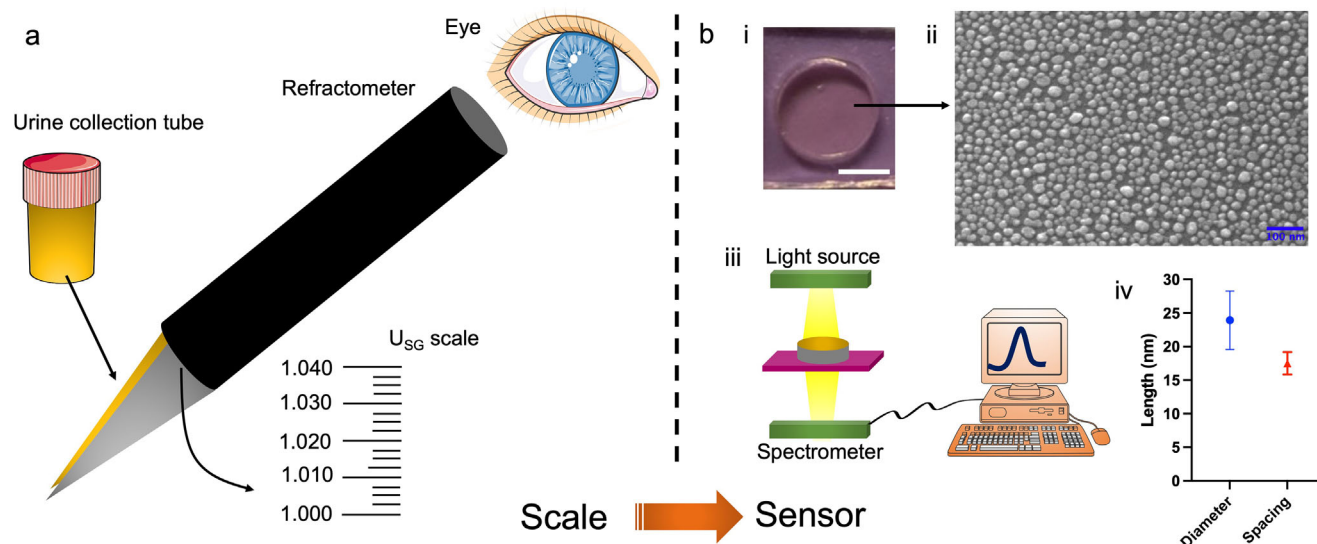


**Figure 1.** Scale to sensor: a) shows a schematic of a refractive index scale for the measurement of urine parameters which involves observation using the human eye. The schematic also shows a urine collection tube. The arrows indicate the location of the scale (drawn not to the scale) and the location where urine is added on the refractometer; b–i). shows a picture of the LSPR sensors, where the length of the scale is 1 cm. ii). shows scanning electron microscopy image of the LSPR sensor surface which is acquired at magnification 200 000X and at 20 kV. iii). shows measurement of schematic and iv. reveals the mean diameter and spacing of the nanoislands on the LSPR sensor surface. Parts of figure a) were drawn by using pictures from Servier Medical Art, licensed under a Creative Commons Attribution 3.0 Unported License.

to enable advanced features including artificial intelligence. In particular, for Specific Gravity (SG) measurement, there are few sensors described in the literature that are based on both optical and electronic transduction methods,<sup>[24–29]</sup> including surface plasmon resonance (SPR) based SG sensor for food analysis developed by me as a co-author of Garifullina et al.<sup>[30]</sup> However, only limited sensors are proposed for  $U_{SG}$ <sup>[24,29]</sup>, and their translation in portable formats, like the handheld refractometers is nontrivial.

Henceforth, in this work, I develop a new biosensor based on the principle of localized surface plasmon resonance (LSPR) for the detection of  $U_{SG}$ . LSPR biosensors work on the principle of changes in the refractive index of the surrounding media and are highly sensitive to small changes in the refractive index of the surrounding medium, which is useful in detecting very low concentrations of analytes.<sup>[31]</sup> LSPR biosensors do not require labeling or modification of the target sample, which simplifies the detection process and reduces the cost of the assay.<sup>[32]</sup> Additionally, it offers features such as real-time monitoring and minimal sample preparation, which reduces the risk of sample degradation and contamination. There are other features of LSPR such as the requirement of small sample volumes, which is particularly important when analyzing precious or limited samples, and the ease of use, which means minimal training is required to operate, making them accessible to a broad range of researchers and clinicians.<sup>[33]</sup> Lastly, with the recent developments in the field of nanofabrication, low-cost LSPR chips are easy to fabricate and the development of portable measurements for LSPR chips is now feasible.<sup>[34]</sup> The developed LSPR sensor in this work is first tested for SG measurement of aqueous solutions followed by detection of  $U_{SG}$ . An uncomplicated test (running experiment) is also performed using LSPR to showcase the superior sensitivity of a sensor over a scale. This experiment highlights the advantage

of using a sensor instead of a scale. The outcomes were analyzed using an unsupervised machine learning algorithm called principal component analysis (PCA). The results demonstrate that it is possible to automate and add artificial intelligence to sensors.

## 2. Experimental Section

### 2.1. Materials

Potassium chloride (assay 99%, CAS# 7447-40-7) was purchased from Sigma-Aldrich (Japan). The author used their own urine samples for that work. Deionized (DI) water from an 18.2 MΩ cm<sup>−1</sup> Milli-Q Integral 3 water purification system (Millipore, Germany) was used as a reference solution, a washing buffer, and a rinsing solution. MASTER-SUR/ $N\alpha$  clinical refractometer (ATAGO CO., LTD, Japan) was used for measuring/calibrating the urine-specific gravity and protein serum. Falcon tubes of 50 mL were purchased from Scientific Fisher

### 2.2. Sensor Fabrication

Using electron beam vapor deposition equipment (KE604TT1-TKF1, Kawasaki Science) in a class 1000 clean room a 4 nm gold (Au) film was deposited at a rate of 0.3 nm<sup>−1</sup> s. The sample was then annealed at 560 °C for 3 h, generating a distribution of Au NIs across the surface of the substrate.

### 2.3. Scanning Electron Microscopy

A small part of the LSPR substrate was cut from the as-deposited nanostructured substrate using a diamond-tipped glass cutter

and attached to a scanning electron microscope (SEM), FEI Quanta 250 FEG mount using carbon tapes. SEM measurements were taken at 20 eV to obtain high-resolution images with a magnification of 200 kX. To compute the size and spacing of the nanoislands, built-in functions of image analysis software ImageJ were used, similar to the analysis in my previous works.<sup>[31–33]</sup>

#### 2.4. Sample Preparation and Measurement

For each of the SG measurements, six sets of aqueous solutions containing KCl where the salt concentration was varied from 100 to 600 mg in 3 mL of water. The SG values were measured using a specific gravity meter (Anton Paar DMA 35 Ex, Japan), also used in the author's previous work to calibrate SG solutions.<sup>[30]</sup> To measure the  $U_{SG}$ , the urine sample was collected using falcon tubes (soon after running 10 km in the case of running experiment), and kept at room temperature for 3 h before measurement of  $U_{SG}$  using both refractometer and LSPR sensor.

#### 2.5. Instrumentation

The setup used to study the LSPR response was custom-built by combining discrete optical components necessary for illumination and collection of light from the sample. The setup is similar to the setups used in my several LSPR works of the past.<sup>[31,32]</sup> Briefly, the assembly involves two fiber optics patch cords, one connected with a halogen light source (LS-1-LL) and the other connected to a spectroscope (USB4000-UV-VIS-ES), which were all purchased from Ocean Optics (now Ocean Insight). The RTL-T stage acquired from Ocean Optics was used to align the fiber optics for both light exposure and light collection in the transmission setup. Prior to capturing any signals from the spectroscope, the system underwent calibration in both dark and light spectrum modes. Using the Ocean-View software, which is a cross-platform operating software for spectroscopy also from Ocean Optics, the wavelength dependence of the light absorbed by nanostructures was observed and recorded in an absorption mode to detect the LSPR signal.

#### 2.6. Statistical Analysis

The author conducted Principal Component Analysis (PCA) using the multiple variable analysis tool in GraphPad Prism 10. To select the PC, the classical method based on the Kaiser–Guttman rule was employed, which involves creating uncorrelated principal components from the initial variables. This compression was achieved using orthogonal eigenvectors that capture the maximal amount of variance in the data set, resulting in a smaller number of components that describe the most variation in the data with minimal loss of information. The author's approach assumes that the variance of each original variable was standardized to one. To identify significant PCs, The author considered those with an eigenvalue greater than one, which contains more variance than a single variable in the original data. The author also checked that selected components account for at least 90% of the total variance. For statistical analysis, the author used Pearson

correlation linear regression fit to calculate the correlation matrix between variables. A two-tailed test with a 99% confidence interval was employed to compute the  $p$ -value, where 1 or 0 represents a perfect or no correlation, respectively, values between 0 and 1 represent a concurrent increase or decrease of two variables, and values from  $-1$  to 0 shows an inverse relationship between the two variables. Within Figures 2–4 the experimental data is used as read/recorded from the scale/sensor and no preprocessing is performed. The data presented within these figures with the help of error bars correspond to mean data  $n \geq 3$  with standard deviations.

### 3. Results and Discussion

A schematic representing a traditional refractive index scale for  $U_{SG}$  is shown in Figure 1a. Here the measurements are performed by reading the scale using the naked eye. On the other hand, Figure 1b–i shows the LSPR sensor consisted of gold nanoisland-type structures. The range of nanoisland size varies from  $\approx 19$  to 28 nm with an average size of 23.9 nm. The spacing varies from  $\approx 15$  to 20 nm with an average spacing of 17.5 nm. The SEM of the LSPR sensor surface, schematic of the measurement setup, and the statistics on nanoisland size (diameter and spacing) are shared in Figure 1–ii–iv, respectively.

To test the LSPR sensor for SG, I first prepared aqueous solutions of different SG by mixing varied amounts of KCl in water. By changing the concentration of the given analyte in the solution, one can alter the density and, consequently, the SG value of a given solution. LSPR spectra, as shown in Figure 2a, were acquired for these solutions of different SG. Within these LSPR spectra, a red shift in the LSPR peak wavelength and an increase in the peak absorbance were observed, see Figure 2b. This increase in peak absorbance and peak wavelength was found to be linear in nature. In Figure 2b, the linear curve depicting the absorbance shift has a slope of 0.36, and the linear fit indicating wavelength shifts is 24.04. As the wavelengths and absorbance in Figure 2b are plotted against the SG values in the  $x$ -axis, the slopes essentially represent the sensor's sensitivity, and therefore the sensor's sensitivity is claimed as 0.36 a.u.  $SG^{-1}$  and 24.04 nm  $SG^{-1}$  for absorbance and wavelength changes respectively.<sup>[35]</sup> Motivated by these observations (successful measurement of SG with the LSPR sensor), I tested the sensor for  $U_{SG}$ .

To measure the  $U_{SG}$ , the urine sample was first exposed to the handheld refractometer, MASTER-SUR/ $N\alpha$  clinical refractometer. After recording the  $U_{SG}$ , the sample was exposed to the LSPR sensor. Please note that to avoid biocontamination, the LSPR sensor was only used one time, i.e., it was not reused after exposure to urine once. From the LSPR spectra recorded, see Figure 3a, I extracted the peak absorbance and wavelength values. These peak values are plotted in Figure 3b where I again observed a linear shift in both wavelength and absorbance, similar to the trend observed for changes in SG of aqueous KCl solution shown earlier in Figure 2. The  $U_{SG}$  sensitivity was found to be 1.887 a.u.  $U_{SG}^{-1}$  and 79.21 nm  $U_{SG}^{-1}$  for absorbance and wavelength changes respectively.

In addition to the  $U_{SG}$ , the clinical refractometer used in this work is also designed for measuring the serum protein in the urine. Therefore, I calibrated the absorbance and wavelength

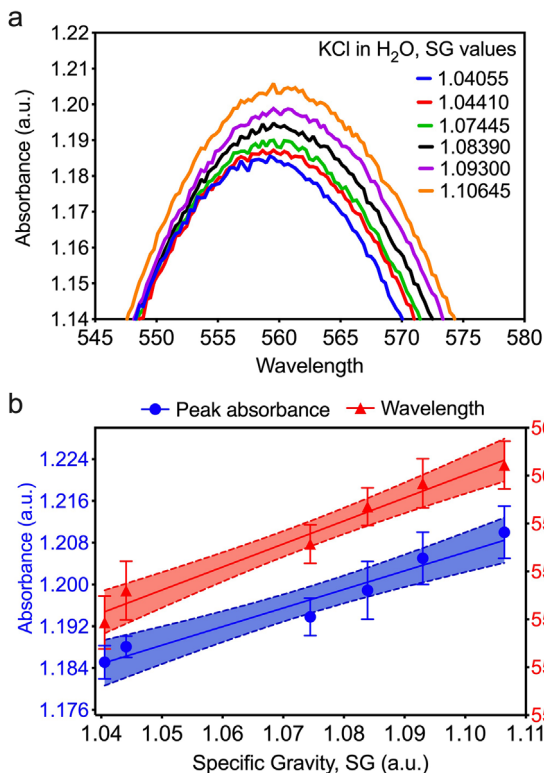


**Figure 2.** Specific Gravity (SG) measurement: a) LSPR spectrum in wavelength versus absorbance plot for different concentrations of KCl in water. The solutions range from 1.04055 to 1.10645 units change in specific gravity; b) change in peak absorbance and LSPR wavelength with respect to changes in the SG. The error bars indicate the standard deviations within experimental repeats ( $n$ ), where  $n \geq 6$ .

shifts of the LSPR spectra obtained for  $U_{SG}$  measurement with the scale of serum protein values in the clinical refractometer. A linear relationship ( $R^2 = 0.99$ ) between  $U_{SG}$  and serum protein was observed from the refractometer, see **Figure 4a**. The wavelength and absorbance shifts are indicated in **Figure 4b**. Ideally, I should have observed  $R^2 = 1$  for the relationship between serum protein and  $U_{SG}$ , since the refractometer is designed with serum protein and  $U_{SG}$  scales are directly proportional to each other. This minute nonlinearity between serum protein and  $U_{SG}$  is attributed to the judgmental error in reading the scale by the user (in this case myself). Such an error can vary from user to user and therefore the reading of  $U_{SG}$  or serum protein is not precise. This is primarily due to the fact that current  $U_{SG}$  measuring portable instruments are mostly based on scales drawn out on glass substrates using refractive index-sensitive prisms.

Such a situation can be aggravated in cases where  $U_{SG}$  or serum protein is required 1.005 to 1.043 units change in specific gravity; b) change in peak absorbance and LSPR wavelength with respect to changes in the  $U_{SG}$ . The error bars indicate the standard deviations within experimental repeats ( $n$ ), where  $n \geq 3$  to be monitored to evaluate an individual's health within the hydrated or dehydrated category. For example, in the literature, a  $U_{SG}$  value of above 1.030 is considered to as dehydrated condition<sup>[36]</sup> and if the user is not able to distinguish small minute changes in the  $U_{SG}$  or for instance reads 1.029 as 1.030 or 1.031 (as it is not easy)

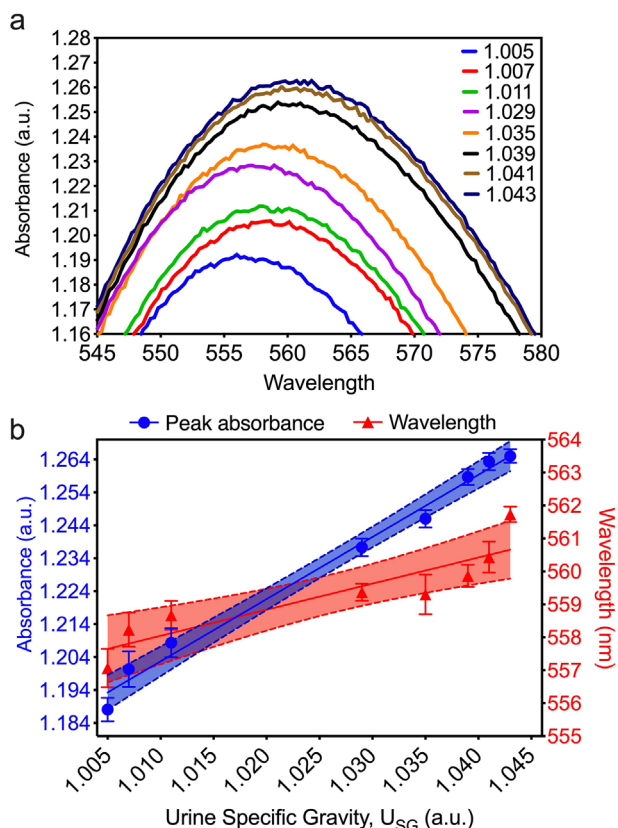


**Figure 3.** Urine Specific Gravity ( $U_{SG}$ ) measurement: a) LSPR spectrum in wavelength versus absorbance plot for different urine samples. The urine samples range from.

one may interpret the hydrated/dehydrated condition incorrectly. In this aspect, an optoelectronic sensor, such as the proposed LSPR sensor, has a clear advantage that will reduce the semantic errors resulting from variation in the reading of the scale from user to user.

To demonstrate this effect, I conducted a simple experiment to compare the LSPR sensor and the MASTER-SUR/ $N\alpha$  clinical refractometer which is specifically designed to measure  $U_{SG}$ . These measurements were conducted by measuring my own urine after running 10 km on different days. The measurement from the LSPR sensor could distinguish four different values of  $U_{SG}$  obtained on 4 different days after four different runs. However, the clinical refractometer is not able to distinguish between these values. See  $U_{SG}$  and serum protein plots in **Figure 4c,d** respectively.

To further evaluate the measurements, I performed principal component analysis (PCA) which is often used as an unsupervised machine learning method in the field of artificial intelligence. PCA is used to find relationships between various features that define a given system. These relationships are further used for eliminating those features (variables) that are redundant to define the system, thereby reducing the complexity of the understanding features of a system. In the context of sensor development, PCA allows for finding co-relationships between the various measurements (such as between absorbance change and wavelength change) in response to a given stimulus. A comprehensive PCA for the SG and  $U_{SG}$  measurements was conducted



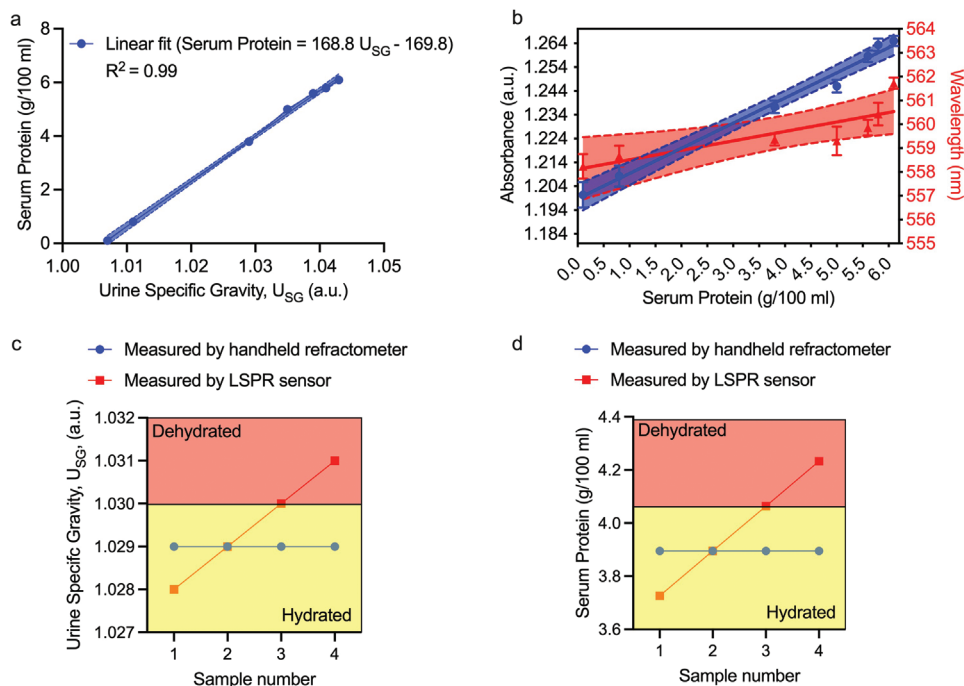


**Figure 4.**  $U_{SG}$  and Serum Protein Characterization: a) Linear fit demonstrating relationship between Serum Protein ( $100 \text{ g mL}^{-1}$ ) and  $U_{SG}$  with  $R^2 = 0.99$ ; b) change in peak absorbance and LSPR wavelength with respect to changes in the Serum Protein ( $100 \text{ g mL}^{-1}$ ); c) Measurements showing LSPR sensor versus refractometer comparison for  $U_{SG}$  detection; d) Measurements showing LSPR sensor versus refractometer comparison for Protein Serum detection in urine samples.

to evaluate the SG and  $U_{SG}$  measuring capabilities of the LSPR system, see **Figure 5**. In this PCA, I attempt to make a qualitative co-relation between seven variables: 1) SG-Theoretical: theoretical value of specific gravity of KCl solutions; 2) SG-LSPR (Abs): Absorbance shifts in the LSPR spectrum when subjected to KCl solutions with different SG values; 3) SG-LSPR (wavelength): Wavelength shifts in the LSPR spectrum when subjected to KCl solutions with different SG values; 4) USG Refractometer: USG measured by clinical refractometer; 5) Serum Protein-Refractometer: Values of serum protein measured by clinical refractometer; 6) USG-LSPR(Abs): Absorbance shifts in the LSPR spectrum when subjected to urine solutions with different SG values; and 7: USG-LSPR (wavelength): Wavelength shifts in the LSPR spectrum when subjected to urine solutions with different SG values. Essentially, these seven variables are correlated by using two principal components (PC1 and PC2) In **Figure 5a**, **1** shows the loading plot, which provides information on how correlated each variable is with that PC. **Figure 5b,c** show the zoomed-in regions of two clusters indicated within **Figure 5a**.

Even though the vectors within the clusters can be resolved, it is clear that there is a difference between the SG measurement in KCl and urine because cluster one exclusively contains values of  $U_{SG}$  and cluster two consists of variables corresponding to SG of KCl. I attribute this to two reasons: 1) the  $U_{SG}$  measured by the LSPR sensor is calibrated by the clinical refractometer in comparison to SG of KCl solutions which is calculated as the relative density of KCl solution with respect to water. Therefore, for SG I am measuring the bulk changes in the refractive index in contrast to the urine sample wherein there is a potential interference of the urine content (serum protein and other electrolytes)

with the nanostructured surface. Since the LSPR sensor is more sensitive to the local changes in the refractive index, the content of urine increases the sensitivity of the LSPR sensor toward the urine sample measured; and 2) The content of the two different samples (urine and KCl solution) offer different ionic surroundings to the nanostructures on the sensor surface where effects resulting from ionic slips, viscosity, and surface tension on the surface results in differences in the sensor response in KCl and urine. Note that some of these aforementioned solid-liquid interfacial effects on transducers are yet to be studied of discovered, let alone be the LSPR surfaces. My recent work reported one such effect on gold nanofilms, liquid slip, which is quantified using quartz crystal microbalance in flow conditions.<sup>[37]</sup>

The associated biplot with the PC scores and loadings is shown in **Figure 5 d,e** shows a scree plot consisting of the ordered PC on the  $x$ -axis, and its corresponding eigenvalues on the  $y$ -axis. The plot also includes the results of Parallel analysis which is a method used to determine the number of PC to retain in the PCA. As per the Kaiser rule, PCs with values greater than one in the data are chosen. This includes PC1 and PC2 which account for 92.30% of the variance in the data as shown in **Figure 5f**. PCA demonstrated in this work is also commonly used in artificial intelligence (AI) applications, especially in the fields of machine learning and deep learning. For instance, in machine learning, PCA can be used to preprocess data by reducing its dimensionality and removing irrelevant features, which can improve the performance and efficiency of subsequent learning algorithms. Furthermore, PCA can be used in the interpretation and visualization of high-dimensional data, which is a key aspect of many AI applications. Within this context, the PCA can be used to

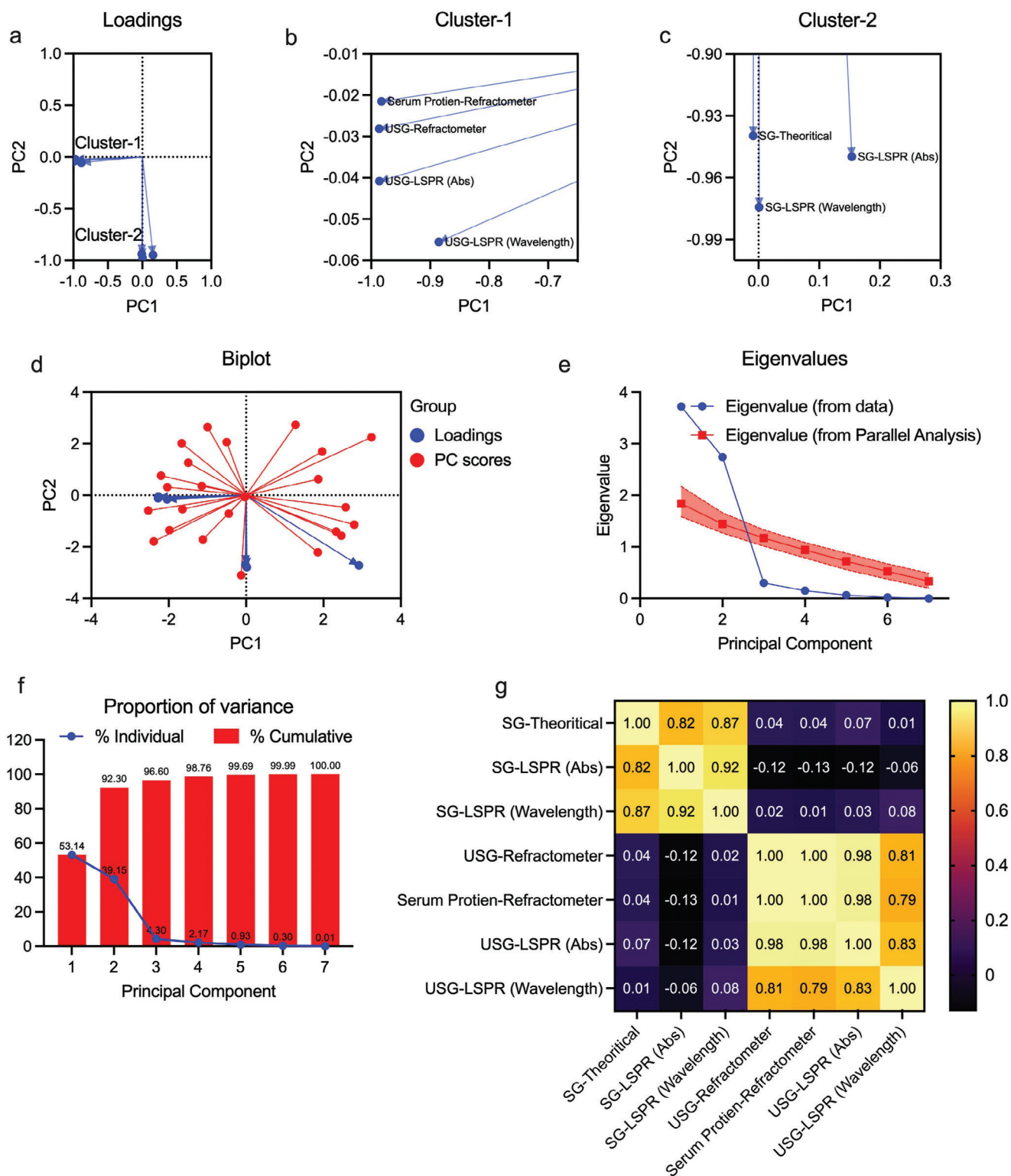


**Figure 5.** Principal component analysis: a) demonstrates the contribution of each principal component toward the variance in the given data; b,c) are zoomed-in versions of cluster one and cluster two shown in (a); d) is the biplot showing loadings and PC scores; e) shows eigenvalues of all principal components d) reveals that principal components one and two account for 92.30% variance, and therefore, PC1 and PC2 are selected to show the loading plot in (a-c); e) shows a matrix showing Pearson correlation ( $r$ ) between all variables used within PCA.

visualize the relationships between different variables or features in a dataset (as demonstrated in this work), which can help to identify patterns and trends in the data, such as measurement differences between buffer or urine samples in this work.

#### 4. Conclusion

In this article, I introduce a straightforward yet effective technique to utilize the highly surface-sensitive optical method called LSPR for measuring  $U_{SG}$ . My study presents an analytical investigation of the interdependence between the Serum Protein and  $U_{SG}$  parameters. By detecting changes in the refractive index, LSPR can indicate changes in the  $U_{SG}$  of a given urine sample. My findings also suggest that traditional LSPR sensors are capable of detecting SG in aqueous solutions. Additionally, the statistical analysis demonstrates that the  $U_{SG}$  sensors have high reproducibility, and employing PCA to analyze the sensing information can potentially lead to intelligent biosensors. The PCA method identifies essential features or variables in a sensor-generated dataset, useful for feature selection or engineering in machine learning applications. Ultimately, the ability to detect  $U_{SG}$  values in a label-free, real-time, and high-throughput manner with reported sensitivity will contribute to an accurate urine monitoring system in the healthcare sector.

#### Acknowledgements

The author would like to thank the support of OIST and in particular Professor Amy Q. Shen, where most of these experiments were conducted during my tenure in her laboratory.

#### Conflict of Interest

The authors declare no conflict of interest.

#### Data Availability Statement

The data that support the findings of this study are available from the corresponding author upon reasonable request.

#### Keywords

biosensors, LSPR, nanoplasmonics, urine-analysis

Received: September 25, 2023

Revised: December 10, 2023

Published online:

[1] D. Zubac, R. Reale, H. Karnincic, A. Sivric, I. Jelaska, *Eur. J. Sport Sci.* **2018**, *18*, 920.

- [2] L. E. Armstrong, J. A. H. Soto, F. T. Hacker, D. J. Casa, S. A. Kavouras, C. M. Maresh, *Int. J. Sport Nutr. Exercise Metab.* **1998**, *8*, 345.
- [3] S. Combs, T. Berl, *Am. J. Kidney Dis.* **2014**, *63*, 294.
- [4] Y. Li, T. Yu, Z. Liu, H. Chen, Y. Liu, Y. Wei, R. Sun, H. Zhang, W. Wang, Y. Lu, *Diabetes Metab. Syndr. Obes.* **2020**, *13*, 4689.
- [5] M. Guo, Q. Chen, Y. Huang, Q. Wu, Y. Zeng, X. Tan, F. Teng, X. Ma, Y. Pu, W. Huang, *Oxid. Med. Cell. Longev.* **2023**, *2023*, 2713864.
- [6] O. Marsenic, *Am. J. Kidney Dis.* **2009**, *53*, 875.
- [7] L. A. Hebert, J. J. Dillon, D. F. Middendorf, E. J. Lewis, J. B. Peter, *Am. J. Kidney Dis.* **1995**, *26*, 432.
- [8] J. Jin, L. Wang, Y. Liu, W. He, D. Zheng, Y. Ni, Q. He, *Front. Endocrinol.* **2022**, *13*, 1018608.
- [9] D. Q. Wang, J. Shuai, H. Zheng, Z. Q. Guo, Q. Huang, X. F. Xu, X. D. Li, H. Zi, D. J. Ming, X. Y. Ren, *Front. Oncol.* **2022**, *11*, 796.
- [10] C. D. Giesen, A. M. Greeno, K. A. Thompson, R. Patel, S. M. Jenkins, J. C. Lieske, *Clin. Biochem.* **2013**, *46*, 810.
- [11] M. J. Steiner, A. L. Nager, V. J. Wang, *Pediatr. Emerg. Care* **2007**, *23*, 298.
- [12] D. M. Minton, E. K. O'Neal, T. M. Torres-McGehee, *J. Athl. Train.* **2015**, *50*, 59.
- [13] S. P. Wyness, J. J. Hunsaker, T. M. Snow, J. R. Genzen, *Pract. Lab. Med.* **2016**, *5*, 65.
- [14] A. de Buys Roessingh, A. Drukker, J. P. Guignard, *Arch. Dis. Child.* **2001**, *85*, 155.
- [15] K. Sumida, G. N. Nadkarni, M. E. Grams, Y. Sang, S. H. Ballew, J. Coresh, K. Mat-sushita, A. Surapaneni, N. Brunskill, S. J. Chadban, *Ann. Intern. Med.* **2020**, *173*, 426.
- [16] I. Saxena, S. Kapoor, R. C. Gupta, *J. Clin. Diagnost. Res.: JCDR* **2013**, *7*, 1846.
- [17] K. Ikeda, M. Abe, I. Masamoto, C. Ishii, E. Arimura, M. Ushikai, K. Oketani, T. Hashiguchi, M. Horiuchi, *Health Sci. Rep.* **2021**, *4*, e267.
- [18] A. Rosinger, *Am. J. Phys. Anthropol.* **2015**, *158*, 696.
- [19] S. B. Su, K. H. Lin, H. Y. Chang, C. W. Lee, C. W. Lu, H. R. Guo, *J. Occupat. Health* **2006**, *48*, 284.
- [20] J. L. Heilesen, J. M. Jayne, *Mil. Med.* **2019**, *184*, e632.
- [21] M. L. Dongare, P. B. Buchade, A. D. Shaligram, *Optik* **2015**, *126* 2383.
- [22] F. Wardenaar, C. P. Ortega-Santos, K. Vento, S. Olzinski, J. Olig, S. Kavouras, C. Johnston, *J. Athl. Train.* **2021**, *56* 389.
- [23] D. W. Ball, *J. Chem. Educ.* **2006**, *83*, 1489.
- [24] N. B. Mustare, *CVR J. Sci. Technol.* **2021**, *20*, 114.
- [25] P. Puligundla, D. Smogrovicova, C. Mok, V. S. R. Obulam, *Innovat. Food Sci. Emerg. Technol.* **2020**, *64*, 102.
- [26] C. W. Lai, Y. L. Lo, J. P. Yur, C. H. Chuang, *IEEE Sens. J.* **2011**, *12*, 827.
- [27] C. Y. Tang, J. T. Lin, *IEEE Sens. J.* **2019**, *20*, 1980.
- [28] C. W. Lai, Y. L. Lo, J. P. Yur, W. F. Liu, C. H. Chuang, *Measurement* **2012**, *45*, 469.
- [29] Y. Chen, Y. Yu, X. Li, H. Zhou, X. Hong, Y. Geng, *Sens. Actuators, B* **2016**, *226*, 412.
- [30] A. Garifullina, N. Bhalla, A. Q. Shen, *Anal. Methods* **2018**, *10*, 290.
- [31] N. Bhalla, S. Sathish, A. Sinha, A. Q. Shen, *Adv. Biosyst.* **2018**, *2*, 1700.
- [32] N. Bhalla, D. Lee, S. Sathish, A. Q. Shen, *Nanoscale* **2017**, *9*, 547.
- [33] N. Bhalla, A. Thakur, I. S. Edelman, R. D. Ivantsov, *ACS Phys. Chem. A* **2022**, *2*, 459.
- [34] N. Bhalla, A. Jamshaid, M. H. Leung, N. Ishizu, A. Q. Shen, *ACS Appl. Nano Mater.* **2019**, *2*, 2064.
- [35] J. Tan, Y. Chen, J. He, L. G. Occhipinti, Z. Wang, X. Zhou, *J. Hazard. Mater.* **2023**, *455*, 131.
- [36] S. Montazer, A. A. Farshad, M. R. Monazzam, M. Eyvazlou, A. A. S. Yaraghi, R. Mirkazemi, *Int. J. Occup. Med. Environ. Health* **2013**, *26*, 762.
- [37] A. F. Payam, B. Kim, D. Lee, N. Bhalla, *Nat. Commun.* **2022**, *13*, 6608.